Mineralogical Magazine, August 2013, Vol. 77(6), pp. 2793–2810

Mineralogy of atmospheric dust impacting the Rio Tinto mining area (Spain) during episodes of high metal deposition

J. C. Fernández-Caliani[1,2,*], J. D. de la Rosa[1,2], A. M. Sánchez de la Campa[2], Y. González-Castanedo[2] and S. Castillo[2]

[1] Departamento de Geología, Facultad de Ciencias Experimentales, Universidad de Huelva, Campus de El Carmen s/n, 21071-Huelva, Spain

[2] Unidad Asociada al CSIC *Contaminación Atmosférica*, Centro de Investigación en Química Sostenible (CIQSO), Universidad de Huelva, Campus de El Carmen s/n, 21071-Huelva, Spain

[*Received 28 May 2013; Accepted 26 June 2013; Associate Editor: K. Hudson-Edwards*]

ABSTRACT

This study is the first to investigate the mineral composition of the atmospheric particulate matter deposited at Rio Tinto, Spain, an historical mining district of world-class importance, with emphasis on metal-bearing particles and their environmental implications. The dustfall is composed of quartz, feldspars, phyllosilicates (mica, chlorite and/or kaolinite) and a variety of accessory heavy minerals, the most common being primary sulfides (pyrite, chalcopyrite with minor galena, sphalerite and bornite) and their oxidation products (notably goethite, hematite and jarosite). This mineral assemblage suggests a local source of wind-blown dust and it is consistent with the large deposition levels of sulfide-related elements (As, Bi, Cd, Cu, Pb, Sb and Zn) registered at the sampling site adjacent to the mine waste dumps. However, the generation of potentially harmful dust particles is not restricted to mine wastes. Anthropogenic metallic compounds arising from a nearby hazardous waste disposal centre can make a relevant additional contribution to the metal deposition, particularly for Fe, Ni, Cr and Mn. Atmospheric fallout is a major mechanism for metal input to soils and plants around or near the mining area.

Keywords: atmospheric dust, bulk deposition, metal-bearing particles, mine wastes, Rio Tinto

Introduction

Atmospheric dispersion of particles from open-cast operations and mine wastes is potentially an important route of human exposure to metals (Plumlee and Morman, 2011). Fugitive dust containing high levels of heavy metals can be transported over long distances (Rasmussen, 1998) away from the mining areas and eventually deposited on the ground when aggregated or washed out by rain, through dry or wet deposition, respectively. As heavy metals present high toxicity and high lability in atmospheric deposition (Golomb *et al.*, 1997), monitoring is important not only in urban and rural areas (Azimi *et al.*, 2003) but also in residential areas adjacent to active and abandoned mines (Roberts and Johnson, 1978; Moreno *et al.*, 2007; Meza-Figueroa *et al.*, 2009; Zota *et al.*, 2009). Atmospheric deposition fluxes of metals and metalloids are required, therefore, in order to evaluate properly the environmental impacts of mine wastes. However, only limited data are available on the ambient air quality at mine sites. A critical review of the literature on the importance of metals and metalloids in dust and

* E-mail: caliani@uhu.es
DOI: 10.1180/minmag.2013.077.6.07

aerosols from mining operations can be found in Csavina *et al.* (2012).

Metalliferous mine wastes containing pulverized material are especially abundant at Rio Tinto (Iberian Pyrite Belt), an historical mining district of world-class importance, both in terms of its ore deposits and environmental geochemistry and mineralogy. Past mining and smelting activities conducted at Rio Tinto (Salkield, 1987), particularly since the middle of the 19th century, left a legacy of huge amounts of hazardous mine wastes that are deposited over extensive areas and subject to leaching and wind-erosion processes. Consequently, airborne metal contaminants may be transferred from erodible waste-rock dumps to surrounding soils and rivers by acid mine-drainage (Galán *et al.*, 2003) and atmospheric deposition of wind-blown dust.

The authors' previous research (Sánchez de la Campa *et al.*, 2011; Castillo *et al.*, 2013) has documented the levels and chemical composition of respirable atmospheric particulate matter (PM_{10}) and atmospheric dustfall (settleable particulate matter), and has estimated the mass contribution of mine wastes to airborne particles using source apportionment techniques. The goal of the present study was to determine the mineralogical profile of the atmospheric deposition impacting the Rio Tinto mining district in order to ascertain: (1) the provenance of settleable metal-bearing particles; (2) the mineral speciation of potentially toxic metals; and (3) their potential detrimental effects on the environment.

Site description

The Rio Tinto mining district is located in Huelva Province of the Autonomous Community of Andalucía, in southwest Spain (Fig. 1), and it encompasses an area of 628 km^2 with a population of ~17,500 people, residing mostly in the villages of Nerva and Minas de Riotinto. The climate is Mediterranean with Atlantic influence, with long dry summers and short mild winters.

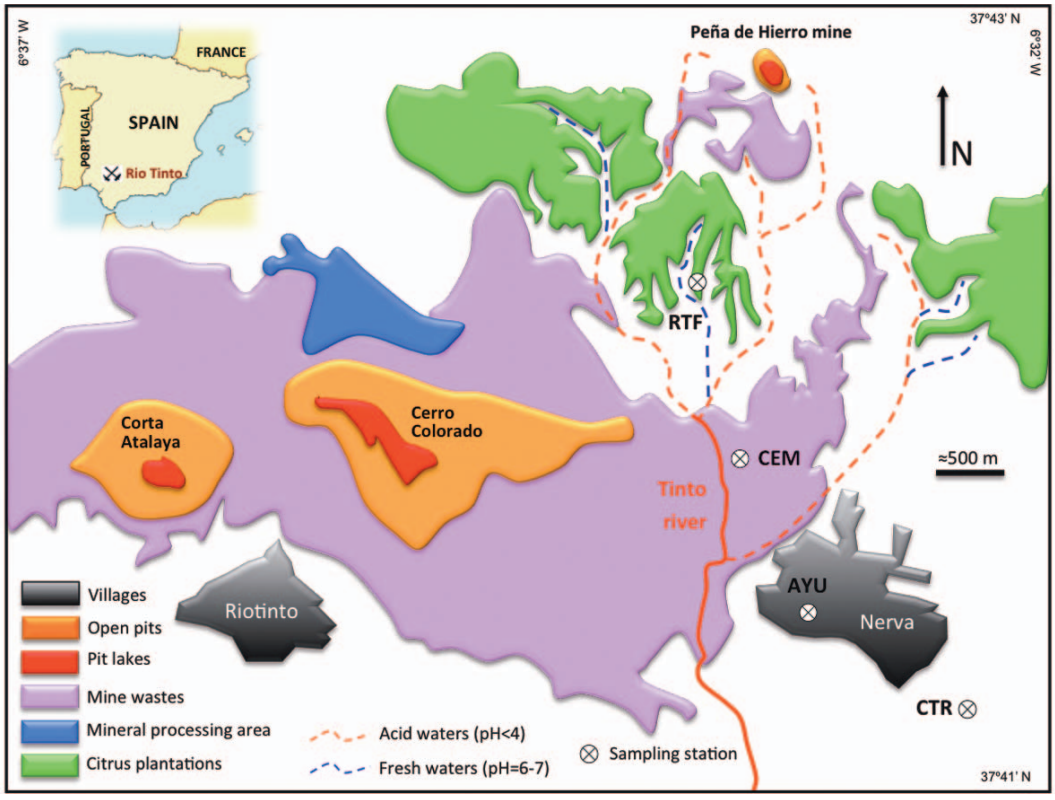

FIG. 1. Generalized map of the Rio Tinto mining district showing land uses and the location of the sampling stations.

The mean annual precipitation is 742 mm and the mean annual temperature is 17.6ºC according to historical weather data recorded by Rio Tinto Co., Ltd. During the period of study (March 2009 to February 2011), the prevailing wind direction in the area was from NW-NNW.

Rio Tinto is regarded as the largest volcanogenic massive sulfide district in the world, with a lengthy history of exploitation that dates back to pre-Roman times, but also represents a notable example of large-scale environmental degradation caused by mining, ore processing and smelting operations (Fernández-Caliani and Galán, 1996; Lottermoser, 2010). For most of the active period, there were few or no regulations concerning the disposal of mine wastes, and so mining activities were carried out without concern or even awareness of their negative environmental impact, resulting in a present-day landscape of large opencasts and voluminous waste-rock dumps, slag deposits, spoil heaps and tailings impoundments which remain untreated (Fig. 2*a*,*b*). The mine was last operated in 2001 due to the low copper price, and it is currently waiting for permission to re-open.

The most widespread waste-rock dumps comprise felsic and mafic volcanic rocks and slates (García-Palomero, 1980), which are made mainly of quartz, feldspars, mica, chlorite, kaolinite and sulfide phases (pyrite with minor chalcopyrite, sphalerite, galena and arsenopyrite) and their secondary weathering products such as hematite, goethite, jarosite and water-soluble efflorescent sulfates (Lottermoser, 2005; Romero *et al.*, 2006). These hazardous materials have the potential for releasing As, Cu, Pb and Zn, among other potentially toxic elements, into the environment (Chopin and Alloway, 2007*a*,*b*; López *et al.*, 2008; Fernández-Caliani *et al.*, 2009). Despite the apparent risk posed by mine wastes, during the last decade many hectares of land around the abandoned mine site have been converted into citrus plantations (Fig. 2*c*).

Materials and analytical methods

Sampling sites and sample collection

Atmospheric bulk deposition (i.e. dry and wet fallout) was collected from March 2009 to February 2011 at four sampling stations (Fig. 1) located in the immediate vicinity of the mine wastes (CEM), in a citrus plantation (RTF), in the urban area of Nerva (AYU) and, lastly, in a truck transfer station near (1 km) a hazardous industrial waste centre (CTR). The sampling locations were chosen to be representative of the land uses of concern and to supply some spatial variability.

Sampling was performed over time periods of 2 weeks using a continuously open bulk deposition collector MCV-PS model, according to the standard test method for collection and measurement of dustfall (ASTM D1739-98/2010). This model consists of a 30.5 cm diameter high-density polyethylene (HDPE) funnel placed at a height of 120 cm above the ground, and connected to a 10 litre HDPE receiving bottle. A nylon mesh ring was mounted around the funnel to avoid contamination by organic debris. The rainwater (wet deposition) was collected and then the funnel was cleaned with Milli-Q water at the end of the sampling periods. In the case of dry deposition, the walls of the funnel were rinsed with 200 ml of Milli-Q water. All samples were subsequently filtered through 0.45 μm silica glass microfibre MUNKTELL filters to separate the soluble and insoluble fractions.

This study focuses on chemical analysis of potentially toxic trace elements in the non-soluble atmospheric particulate matter (32 samples) collected at the four sampling sites during periods of high deposition levels (Table 1), and on mineralogical analysis of the dustfall sampled during the period March 2009–March 2010 in the CEM (26 samples) and RTF (24 samples) stations.

Chemical analysis

The concentrations of major elements and selected trace elements (As, Bi, Cd, Co, Cr, Cu, Ni, Pb, Sb, Se and Zn) were determined after multi-acid digestion of the airborne particles retained in the filters, following the analytical procedure developed by Querol *et al.* (2001). In brief, a half of each filter was digested in closed Teflon PFA reactors with a mixture of HNO_3:HF:$HClO_4$ (1:2:1) at 90ºC. Subsequently, the acidic solution was cooled and dried on a hot plate at 200ºC. The dry residue was re-dissolved in 1.25 ml of HNO_3 and Milli-Q water, and then made up to 25 ml.

Chemical analyses of major and trace elements were done by inductively coupled plasma optical spectrometry (Jobin Yvon ICP-OES) and inductively coupled plasma mass spectrometry (Agilent 7700 Series ICP-MS), respectively. Blank values corresponding to blank MUNKTELL filters were subtracted from measured concentrations. The

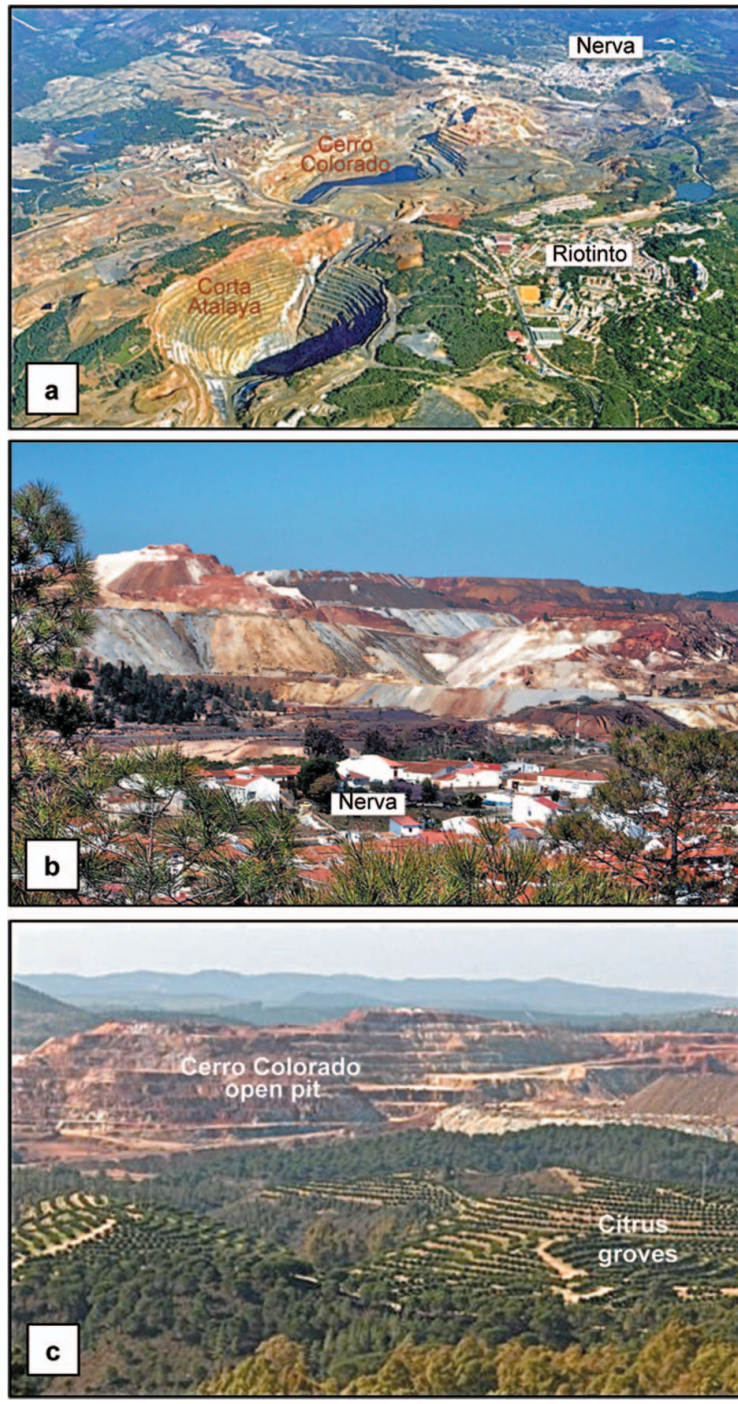

FIG. 2. Panoramic views of the Rio Tinto mining district: (*a*) Corta Atalaya and Cerro Colorado open-pit mines, (*b*) mine waste dumps in the vicinity of the urban area of Nerva and (*c*) citrus plantations surrounding the mining area. Photos courtesy of E. Romero.

TABLE 1. Sample-collection data and weather conditions during sampling periods.

Sampling station	Sample code	Sampling period	Precipitation (l/m^2)	Prevailing wind direction
AYU N37º41′42″ W6º33′03″	S74	27/03/2009 – 13/04/2009	0.0	N
	S151	28/08/2009 – 11/09/2009	0.0	S
	S158	11/09/2009 – 25/09/2009	22.7	S
	S212	18/12/2009 – 04/01/2010	138.2	WNW/SSE
	S322	02/07/2010 – 16/07/2010	0.0	NW/S
	S425	03/01/2011 – 14/01/2011	68.0	WNW/SW/WSW
CEM N37º42′10″ W6º33′26″	S69	12/03/2009 – 27/03/2009	0.0	SSE
	S89	24/04/2009 – 08/05/2009	0.0	SSE/NWN
	S96	08/05/2009 – 22/05/2009	2.6	WSW
	S103	22/05/2009 – 05/06/2009	1.0	WNW/S
	S110	05/06/2009 – 19/06/2009	8.4	NW/SSE
	S152	28/08/2009 – 11/09/2009	0.0	S
	S213	18/12/2009 – 04/01/2010	134.4	WNW/SSE
	S275	12/04/2010 – 26/04/2010	132.6	S
	S323	02/07/2010 – 16/07/2010	0.0	NW/S
	S387	22/10/2010 – 05/11/2010	30.9	S/SSW/SE
CTR N37º41′15″ W6º32′20″	S83	13/04/2009 – 24/04/2009	18.0	NW
	S139	31/07/2009 – 17/08/2009	15.2	NW
	S153	28/08/2009 – 11/09/2009	0.0	S
	S160	11/09/2009 – 25/09/2009	21.9	S
	S190	06/11/2009 – 20/11/2009	0.0	N
	S308	04/06/2010 – 18/06/2010	37.2	NNW/WNW
	S324	02/07/2010 – 16/07/2010	0.0	NW/S
RTF N37º43′08″ W6º33′38″	S105	22/05/2009 – 05/06/2009	2.6	WNW/S
	S112	05/06/2009 – 19/06/2009	9.6	NW/SSE
	S126	03/07/2009 – 17/07/2009	0.0	NWN
	S133	17/07/2009 – 31/07/2009	0.0	WNW/S
	S147	14/08/2009 – 28/08/2009	0.0	NWN/S
	S191	06/11/2009 – 20/11/2009	0.0	N
	S263	12/03/2010 – 26/03/2010	7.7	SSE
	S309	04/06/2010 – 18/06/2010	39.0	NNW/WNW
	S365	10/09/2010 – 24/09/2010	11.4	S/SSE

average precision and accuracy are within the typical range of analytical errors (3−10%) for the elements studied, and were controlled by repeated analysis of a certified reference material (fly ash NBS-1633b).

Mineralogical analysis

The major mineral composition of the non-soluble material was determined by powder X-ray diffraction (XRD) on a BRUKER AXS D8-Advance diffractometer using monochromatic CuKα radiation at 40 kV and 30 mA. The filters were scanned from 3 to 65º 2θ, with a step size of 0.02º and a counting time of 0.6 s per step. Relative mineral abundance was estimated semi-quantitatively by empirical factors weighting the integrated peak areas of distinctive reflections, in combination with the 100% approach (Kahle *et al.*, 2002).

The filters selected for chemical analysis were also examined by scanning electron microscopy (SEM) using a JEOL JSM-5410 instrument operated at 20 kV, and equipped with an energy dispersive X-ray (EDS) analytical system (Oxford Link ISIS). Accessory heavy-metal bearing phases were identified and characterized using

back-scattered electron (BSE) imaging and EDS microanalysis.

Results and discussion

Major and trace elements deposition

The atmospheric (wet plus dry) deposition of major elements during the monitoring periods (Table 2) was characterized by relatively high levels of Al (up to 214 mg/m^2), Fe (up to 178 mg/m^2) and minor amounts of the other elements. The largest mass deposition levels of Al and Fe were measured at the sampling station nearest the mining area (CEM). This station also registered the maximum concentration of S (29 mg/m^2), while the highest levels of Ca (136 mg/m^2) and P (54 mg/m^2) were deposited in the urban station (AYU).

The atmospheric deposition also contained relatively high levels of some trace elements, such as Zn (up to 8.44 mg/m^2), Pb (up to 7.48 mg/m^2), Cu (up to 6.16 mg/m^2), Sb (up to 2.41 mg/m^2) and As (up to 1.36 mg/m^2) in comparison with other metals and metalloids (Table 3). These potentially toxic elements along with Fe and S are typical components of the major sulfides present in the mine wastes (Romero *et al.*, 2006), and denote the chemical profile of the atmospheric particulate matter influenced by the mining source (Castillo *et al.*, 2013).

The largest mean deposition values (Fig. 3) of Pb (1.63 mg/m^2), As (0.44 mg/m^2) and Sb (0.34 mg/m^2) were registered at the CEM station, which is located just in the prevailing wind direction, and so exposed to wind-blown dust from the mine wastes. It is noticeable the relatively large deposition levels of Pb (7.48 mg/m^2), Zn (3.34 mg/m^2), Cu (2.27 mg/m^2), Sb (2.41 mg/m^2), As (1.36 mg/m^2), Bi (0.42 mg/m^2), Se (0.16 mg/m^2) and Cd (0.13 mg/m^2) in the dustfall collected at the CEM station occurred between 24 April and 22 May 2009.

Nevertheless, it was found that the highest mean deposition values of Zn (2.85 mg/m^2), Cr (0.19 mg/m^2) and Ni (0.09 mg/m^2) as well as high levels of Pb (0.61 mg/m^2 on average) were deposited by the prevailing wind at the CTR sampling station (Fig. 3). This fact could be related to the additional combined contribution of the traffic, road dust and waste disposal operations to air pollution, as CTR was located in a truck transfer station in close proximity to an industrial waste centre.

In general, the median levels of atmospheric metal deposition registered at the AYU and RTF

TABLE 2. Atmospheric deposition of major and minor elements (in mg/m^2) during the sampling intervals (2 weeks) considered in the present study.

Sampling stations	Sampling periods	Al	Ca	Fe	K	Mg	Mn	Na	P	Ti	S
AYU	27/03/2009–13/04/2009	22	4.7	14	5.8	3.0	0.3	2.1	0.1	1.6	<0.1
	28/08/2009–11/09/2009	19	14	14	5.1	3.3	0.2	2.1	1.0	1.3	0.6
	11/09/2009–25/09/2009	21	2.9	2.8	5.5	2.8	0.3	1.9	0.9	1.6	0.7
	18/12/2009–04/01/2010	115	8.2	27	35	20	1.0	13	9.6	13	12
	02/07/2010–16/07/2010	46	136	43	19	13	0.8	6.1	54	4.5	4.4
	03/01/2011–14/01/2011	92	9.4	94	28	11	0.6	2.9	2.1	9.1	5.2
	Mean	52.7	29.3	32.5	16.5	8.8	0.5	4.7	11.2	5.2	3.8
	Median	34	8.8	20.5	12.4	7.2	0.5	2.5	1.6	3.1	2.6
	Stand. Dev.	41.4	52.6	33.3	13.1	6.9	0.3	4.4	21.1	5.0	4.5

	12/03/2009–27/03/2009	20	5.0	17	5.3	4.3	0.2	1.5	0.1	2.0	<0.1
	24/04/2009–08/05/2009	148	23	178	44	12	0.7	9.7	2.1	10	0.1
	08/05/2009–22/05/2009	214	44	165	63	29	1.6	11	1.3	31	0.4
	22/05/2009–05/06/2009	18	2.9	21	5.2	2.1	0.1	1.6	0.3	1.2	<0.1
	05/06/2009–19/06/2009	27	2.7	22	6.9	3.4	0.2	2.0	0.2	1.6	<0.1
	28/08/2009–11/09/2009	15	3.4	3.3	3.8	2.4	0.2	1.6	0.3	1.0	0.8
CEM	18/12/2009–04/01/2010	102	7.8	20	29	14	0.6	7.9	5.9	10	29
	12/04/2010–26/04/2010	17	2.6	17	9.0	4.2	<0.1	4.7	9.7	1.3	5.7
	02/07/2010–16/07/2010	22	6.6	21	7.8	5.5	0.4	2.2	0.5	1.7	0.8
	22/10/2010–05/11/2010	92	8.0	94	18	7.2	0.5	6.2	1.8	5.5	11
	Mean	67.5	10.6	55.8	19.2	8.5	0.5	4.9	2.2	6.6	4.8
	Median	24.5	5.8	21	8.4	4.9	0.3	3.5	0.9	1.9	0.6
	Stand. Dev.	69.5	13.1	65.7	20.1	8.4	0.5	3.7	3.1	9.3	9.3
	13/04/2009–24/04/2009	54	8.9	40	17	7.8	1.0	9.1	0.6	4.6	<0.1
	31/07/2009–17/08/2009	49	4.2	4.2	12	5.7	0.8	5.8	1.3	3.0	1.2
	28/08/2009–11/09/2009	29	14	14	7.8	4.2	0.5	4.8	0.6	1.7	0.5
	11/09/2009–25/09/2009	25	2.0	1.9	7.4	2.7	0.4	3.5	0.7	1.4	0.6
	06/11/2009–20/11/2009	8.8	3.0	3.1	2.2	1.8	0.1	1.4	0.2	1.1	0.1
CTRA	04/06/2010–18/06/2010	65	12	63	22	8.7	1.2	11	4.7	4.0	5.1
	02/07/2010–16/07/2010	29	17	27	9.5	7.3	0.7	3.7	0.6	2.9	0.7
	Mean	37.1	8.7	21.8	11.2	5.5	0.7	5.6	1.2	2.7	1.2
	Median	29	8.9	14	9.5	5.7	0.7	4.8	0.6	2.9	0.6
	Stand. Dev.	19.6	5.8	22.9	6.5	2.6	0.4	3.4	1.6	1.3	1.8
	22/05/2009–05/06/2009	24	4.0	16	10	4.8	0.3	1.6	0.1	1.8	0.1
	05/06/2009–19/06/2009	53	3.0	31	14	7.5	0.3	3.1	0.2	3.8	0.1
	03/07/2009–17/07/2009	13	2.2	7.0	3.4	1.5	3.7	1.5	0.1	1.0	<0.1
	17/07/2009–31/07/2009	22	3.0	11	5.1	2.9	0.7	1.7	0.1	1.4	<0.1
	14/08/2009–28/08/2009	15	2.4	2.3	3.9	2.0	0.4	1.5	0.5	1.0	1.8
	06/11/2009–20/11/2009	12	3.7	3.8	3.8	2.1	0.1	1.3	0.2	1.6	1.0
RTF	12/03/2010–26/03/2010	40	12	40	18	16	0.5	4.4	2.7	3.0	1.9
	04/06/2010–18/06/2010	62	7.1	59	34	13	9.4	6.8	22	5.2	13
	10/09/2010–24/09/2010	71	7.6	74	25	15	4.7	9.8	3.9	5.5	3.7
	Mean	34.5	5.0	27.2	13.1	7.1	2.2	3.5	3.3	2.7	2.4
	Median	24	3.7	16	10	4.8	0.5	1.7	0.2	1.8	1.0
	Stand. Dev.	22.5	3.2	25.8	10.9	5.9	3.2	3.0	7.2	1.8	4.1

TABLE 3. Atmospheric deposition of selected trace elements (in mg/m^2) during the sampling intervals (2 weeks) considered in the present study.

Sampling station	Sampling periods	Cr	Co	Ni	Cu	Zn	As	Se	Cd	Sb	Pb	Bi
AYU	27/03/2009–13/04/2009	0.02	0.04	0.02	0.12	0.41	0.04	<0.01	<0.01	0.01	0.12	<0.01
	28/08/2009–11/09/2009	0.01	0.03	<0.01	0.12	0.26	<0.01	<0.01	<0.01	<0.01	0.03	<0.01
	11/09/2009–25/09/2009	<0.01	0.02	<0.01	0.16	0.53	<0.01	<0.01	<0.01	<0.01	0.02	<0.01
	18/12/2009–04/01/2010	0.13	0.22	0.08	1.35	2.46	0.14	0.05	<0.01	0.08	1.06	0.01
	02/07/2010–16/07/2010	0.11	0.06	0.07	0.34	1.21	0.05	0.01	0.01	0.01	0.23	<0.01
	03/01/2011–14/01/2011	0.50	0.06	0.10	0.82	1.49	0.05	<0.01	<0.01	0.01	0.17	0.07
	Mean	0.13	0.07	0.05	0.49	1.06	0.05	0.01	<0.01	0.02	0.27	0.02
	Median	0.07	0.05	0.05	0.25	0.87	0.05	<0.01	<0.01	0.01	0.15	<0.01
	Stand. Dev.	0.19	0.07	0.04	0.50	0.84	0.05	0.02	0.00	0.03	0.39	0.03
CEM	12/03/2009–27/03/2009	0.03	0.04	0.02	0.08	0.43	0.04	0.02	0.01	0.01	0.08	<0.01
	24/04/2009–08/05/2009	0.09	0.05	0.05	2.27	3.13	0.64	0.05	0.06	2.41	7.48	0.42
	08/05/2009–22/05/2009	0.39	0.15	0.35	1.95	3.34	1.36	0.16	0.13	0.33	2.39	0.13
	22/05/2009–05/06/2009	0.02	0.01	0.01	0.27	0.25	0.22	<0.01	<0.01	0.06	0.37	0.02
	05/06/2009–19/06/2009	0.03	0.02	0.01	0.24	0.45	0.19	0.01	<0.01	0.05	0.30	0.02
	28/08/2009–11/09/2009	0.04	0.02	0.02	0.10	0.21	0.10	0.01	<0.01	0.02	0.16	0.01
	18/12/2009–04/01/2010	0.18	0.12	0.11	1.39	1.95	0.97	0.20	<0.01	0.28	3.39	0.10
	12/04/2010–26/04/2010	0.01	0.01	<0.01	1.09	0.68	0.19	<0.01	0.02	0.04	0.40	0.01
	02/07/2010–16/07/2010	0.05	0.02	0.02	0.09	0.26	0.04	<0.01	<0.01	0.02	0.11	<0.01
	22/10/2010–05/11/2010	0.07	0.05	0.03	1.09	0.95	0.70	0.01	<0.01	0.21	1.59	0.07
	Mean	0.09	0.05	0.06	0.86	1.17	0.45	0.05	0.03	0.34	1.63	0.08
	Median	0.05	0.03	0.02	0.68	0.57	0.21	0.01	<0.01	0.06	0.39	0.02
	Stand. Dev.	0.12	0.05	0.11	0.82	1.21	0.45	0.07	0.04	0.74	2.35	0.13
CTR	13/04/2009–24/04/2009	0.29	0.03	0.14	0.70	5.66	0.10	<0.01	<0.01	0.02	1.61	0.02
	31/07/2009–17/08/2009	0.11	0.01	0.06	0.26	2.83	0.03	<0.01	<0.01	0.01	0.43	0.01
	28/08/2009–11/09/2009	0.05	<0.01	0.03	0.17	1.54	0.02	<0.01	<0.01	<0.01	0.25	<0.01
	11/09/2009–25/09/2009	0.07	0.01	0.03	0.13	1.19	0.02	<0.01	<0.01	<0.01	0.29	<0.01
	06/11/2009–20/11/2009	0.05	0.03	0.03	0.04	0.09	0.02	<0.01	<0.01	0.01	<0.01	<0.01
	04/06/2010–18/06/2010	0.61	0.08	0.25	0.76	6.27	0.10	0.01	0.04	0.04	1.36	0.04
	02/07/2010–16/07/2010	0.16	0.03	0.07	0.18	2.34	0.04	<0.01	0.05	0.01	0.35	0.01
	Mean	0.19	0.03	0.09	0.32	2.85	0.05	<0.01	0.02	0.01	0.61	0.01
	Median	0.11	0.03	0.06	0.18	2.34	0.03	<0.01	<0.01	0.01	0.35	0.01
	Stand. Dev.	0.20	0.03	0.08	0.29	2.31	0.04	0.00	0.02	0.01	0.61	0.01

RTF	22/05/2009–05/06/2009	0.03	0.01	0.01	0.22	1.02	0.06	0.02	<0.01	0.01	0.15	<0.01
	05/06/2009–19/06/2009	0.07	0.02	0.03	0.23	0.83	0.06	0.02	<0.01	0.01	0.18	<0.01
	03/07/2009–17/07/2009	<0.01	<0.01	<0.01	0.06	0.03	<0.01	<0.01	<0.01	<0.01	0.01	<0.01
	17/07/2009–31/07/2009	<0.01	<0.01	<0.01	0.10	0.33	<0.01	<0.01	<0.01	<0.01	0.01	<0.01
	14/08/2009–28/08/2009	0.01	<0.01	0.01	0.06	0.11	0.01	<0.01	<0.01	<0.01	0.03	<0.01
	06/11/2009–20/11/2009	0.02	0.02	0.01	1.17	2.26	0.02	<0.01	<0.01	<0.01	0.05	<0.01
	12/03/2010–26/03/2010	0.07	0.02	0.02	6.16	0.31	0.02	<0.01	<0.01	0.01	0.05	<0.01
	04/06/2010–18/06/2010	0.23	0.25	0.18	<0.01	8.44	0.11	0.01	<0.01	0.02	0.62	0.02
	10/09/2010–24/09/2010	0.13	0.10	0.07	0.32	2.42	0.05	<0.01	<0.01	0.01	0.32	<0.01
	Mean	0.06	0.05	0.04	0.93	1.75	0.04	<0.01	<0.01	<0.01	0.16	<0.01
	Median	0.03	0.02	0.01	0.22	0.83	0.02	<0.01	<0.01	0.01	0.05	<0.01
	Stand. Dev.	0.07	0.08	0.06	1.99	2.66	0.04	0.01	0.00	0.00	0.20	0.01

monitoring stations were low compared with those found at CEM and CTR, although it must be noted the elevated concentrations of Cu (6.16 mg/m^2) and Zn (8.44 mg/m^2) were deposited at RTF during the sampling periods 12–26 March 2010 and 4–18 June 2010, respectively. This collector was situated on citrus grove soils subjected to fertilizer and pesticide application during spring months.

Mineral composition

The mineral assemblage identified by XRD in the dustfall comprises essentially quartz, feldspars, dioctahedral mica (muscovite/illite), and phyllosilicates with a basal spacing of 7 Å (kaolinite and chlorite), although conspicuous amounts of goethite were also present in some samples. The mineral composition is consistent with the chemistry of the atmospheric deposition in terms of major elements.

Mica and chlorite occurred as partly pseudohexagonal plates ranging up to 50 μm in size, while kaolinite appeared as smaller flakes with irregular edges. In addition, the SEM-BSE observations and EDS microanalyses (Fig. 4) implied the occurrence of accessory phases, such as hematite, jarosite, baryte, apatite, gypsum, ilmenite, rutile, titanite, cassiterite, zircon, monazite and a variety of metal-bearing sulfides that will be described in detail later. The subordinate minerals usually exhibit irregular shapes and particle sizes smaller than 10 μm, although hematite also occurred as pseudomorphs after cubic crystals of pyrite.

The mineral composition of the dust that settled on the CEM and RTF collectors showed some differences in terms of quantitative mineral abundance (Fig. 5). In comparison, the content of quartz in CEM (25–55%) was greater than in RTF (10–45%), thus reflecting the influence of nearby quartz-rich waste rocks (the locally so-called Tejonera mine wastes). The dustfall collected at the RTF rural station is composed mainly of mica with minor amounts of kaolinite and chlorite, which globally accounted for more than 60% of the bulk mineral composition in most samples. In this case, the dominance of phyllosilicates is attributed to resuspension of clay minerals derived from the surrounding shales and soils under citrus production. Carbonate minerals were not detected either by XRD or SEM-EDS, which is consistent with a general lack of carbonate sources in the region. Therefore, the

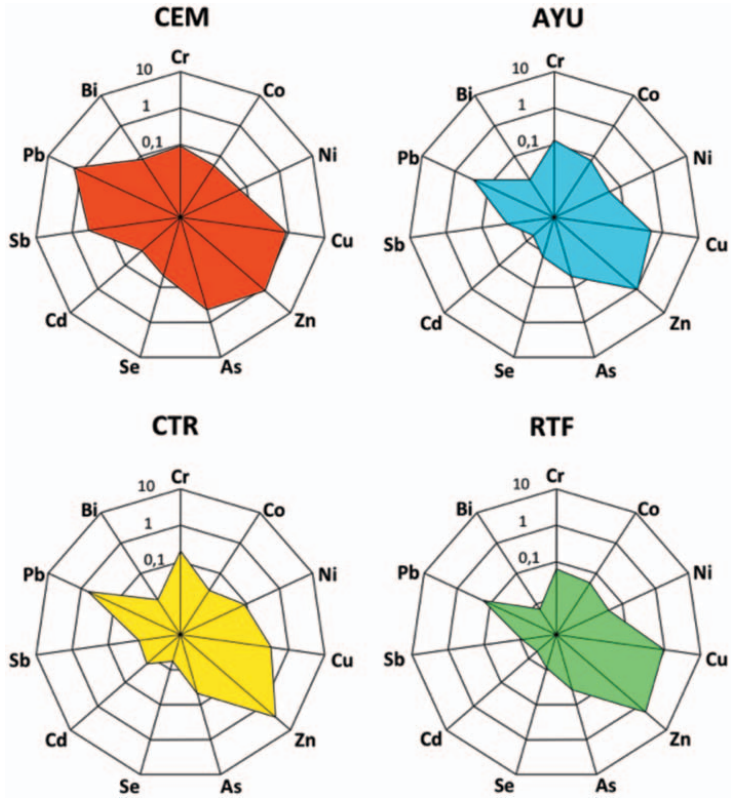

FIG. 3. Spider charts displaying the mean values of trace elements at each sampling location.

mineral composition is mainly controlled by the source-area lithology, and largely reflects the terrigenous character of the dustfall. Temporal variation in mineral abundance may be related to changes in the prevailing wind direction.

Besides the minerals mentioned above, the atmospheric deposition samples also contain fly-ash particles from fossil fuel combustion, small fragments of fayalitic slags from ancient smelting operations, and abundant pollen grains.

Mineralogy of metal-bearing particles

The following heavy metal-hosting particles were identified from the SEM-EDS study: primary sulfides, secondary minerals formed by weathering of primary sulfides and metallic compounds of anthropogenic origin.

Primary sulfides

Pyrite and chalcopyrite were by far the most common primary sulfides found in the samples examined. In fact, a large number of relatively coarse individual particles of pyrite and chalcopyrite, mainly in the 20–30 μm grain-size range, were present in the mineral dust collected, particularly at CEM, thereby accounting for the high levels of metal deposited on this sampling site. Abundance of coarse particles of metal-bearing sulfides in the collector closest to mine wastes suggests a local source area. The airborne metal-bearing particles collected at AYU and RTF stations were essentially the same as at CEM in shape and mineral composition, but they were smaller in size (up to 10 μm).

Pyrite occurred frequently as well formed cubic crystals (Fig. 6*a*,*b*) showing extensive development of surface etch pits and microvoids arising from oxidative dissolution, while chalcopyrite usually appeared as irregularly shaped angular particles (Fig. 6*c*). Other primary base-metal sulfides and sulfosalts were more rarely seen, such as galena (Fig. 6*d*), sphalerite, bornite (Fig. 6*e*) and a lead-antimony sulfosalt (Fig. 6*f*),

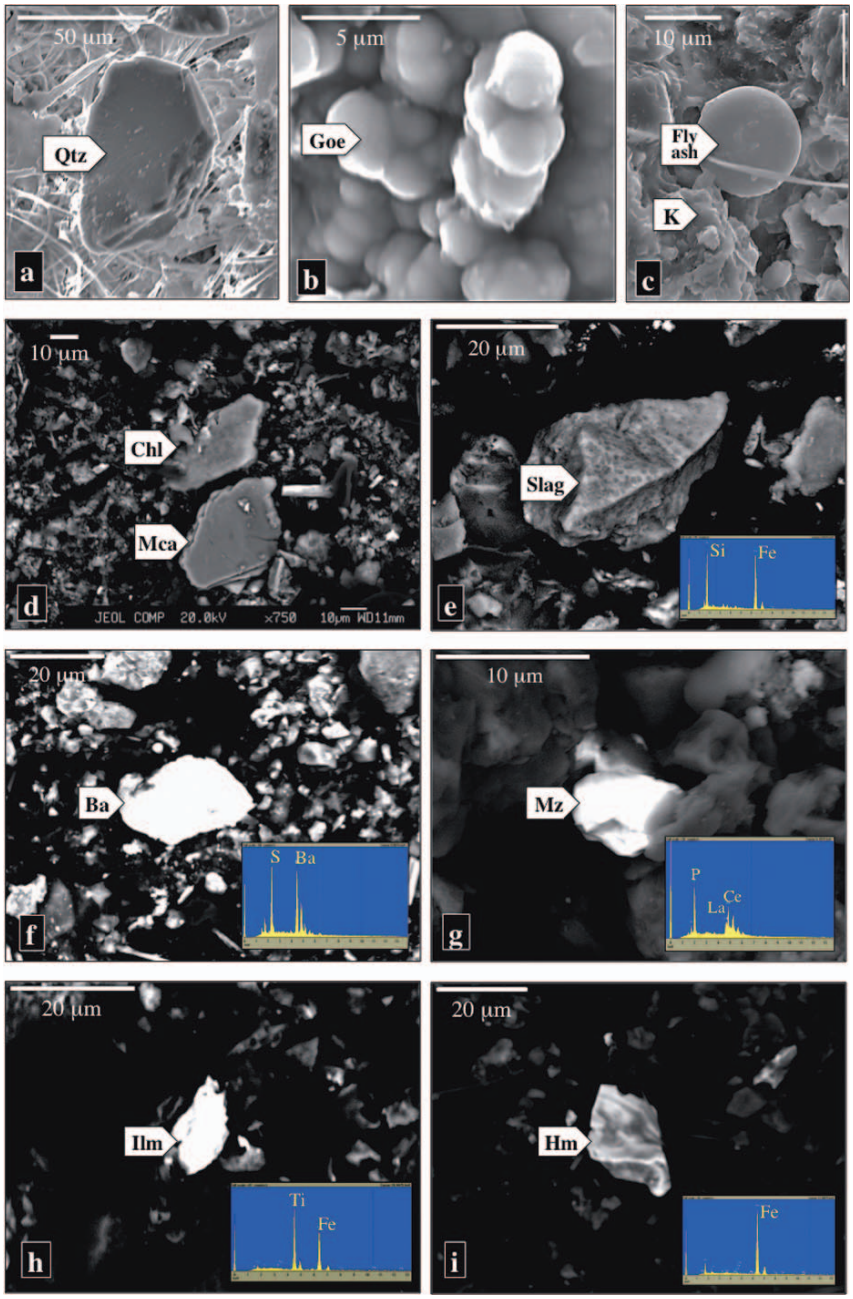

FIG. 4. SEM images and EDS spectra of some minerals commonly occurring in the dustfall: (*a*) subhedral crystal of quartz; (*b*) botryoidal aggregates of goethite; (*c*) aggregates of kaolinite flakes surrounding a fly-ash particle with a smooth spherical surface; (*d*) platy subhedral crystals of muscovite and chlorite; (*e*) slag particle of fayalitic composition; (*f*) tabular orthorhombic crystal of baryte; (*g*) isolated particle of monazite, a light rare earth element-bearing phosphate; (*h*) individual particle of ilmenite; (*i*) particle of iron oxide, probably hematite pseudomorphs after pyrite. Mineral abbreviatons: Ba: baryte, Chl: chlorite, Goe: goethite, Hm: hematite, Ilm: ilmenite, K: kaolinite, Mz: monazite, Mca: muscovite, Qtz: quartz.

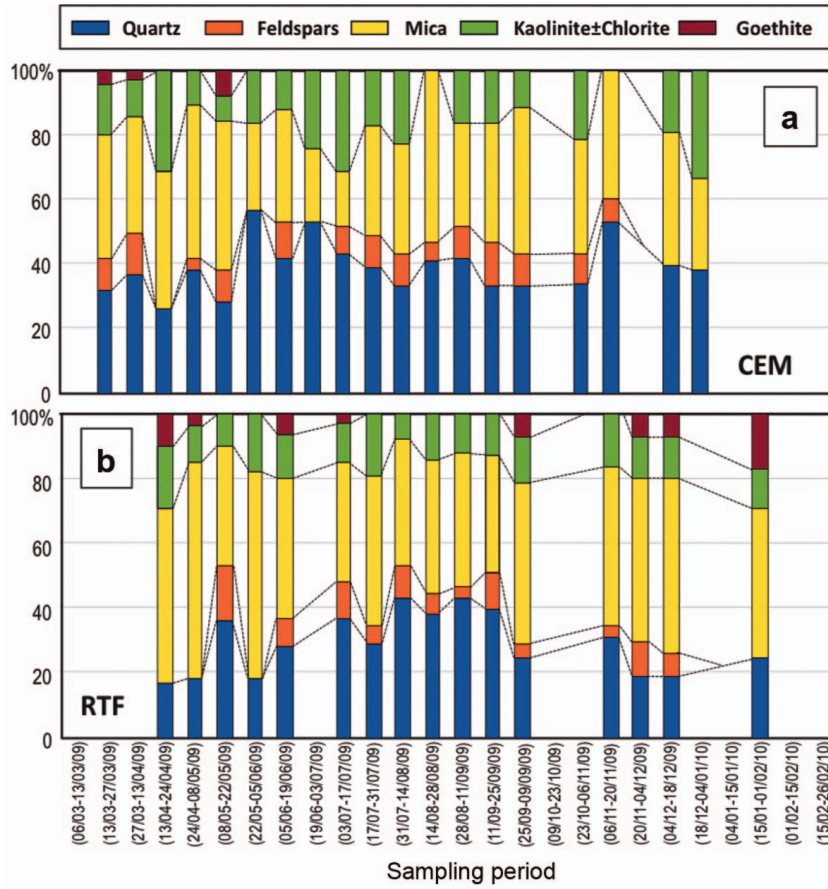

FIG. 5. Time evolution of the mineralogical composition of the dustfall samples collected at the CEM (*a*) and RTF (*b*) monitoring stations.

which is probably boulangerite ($Pb_5Sb_4S_{11}$), although too small for certain identification. These phases occurred as anhedral rounded particles generally <5 μm in size.

Secondary minerals formed by weathering of primary sulfides

A number of secondary phases that occur typically in the oxidation and supergene enrichment zones of the copper ore deposits of Rio Tinto (García-Palomero, 1980) have been identified in some filters, including oxides (hematite, goethite, cuprite, delafossite), sulfates (jarosite) and copper sulfides, probably chalcocite or covellite (Fig. 7).

Hematite and goethite were found to be the most common secondary minerals in the settleable particulate matter, however almost all the particles of iron oxy-hydroxides that were analysed by SEM-EDS did not have detectable levels of heavy metal(loid)s. Exceptionally, some granular aggregates made up of iron oxide particles bearing Sb and Bi were detected in samples from the CEM collector. Minor amounts of copper oxide particles (such as cuprite), which occurred as clusters of tiny particles (<5 μm in size), were also recognized in several samples from the same collector. Particles of a copper-iron oxide measuring up to 20 μm were ascribed to delafossite ($CuFeO_2$).

Another typical secondary mineral widely found in the dustfall samples is jarosite, a basic hydrous sulfate ($KFe_3[SO_4]_2[OH]_6$) occurring naturally at the Rio Tinto mining area (Fernández-Remolar *et al.*, 2011). Two distinct types of jarosite particles were distinguished based on morphological and compositional differences. Jarosite appeared as fine tabular

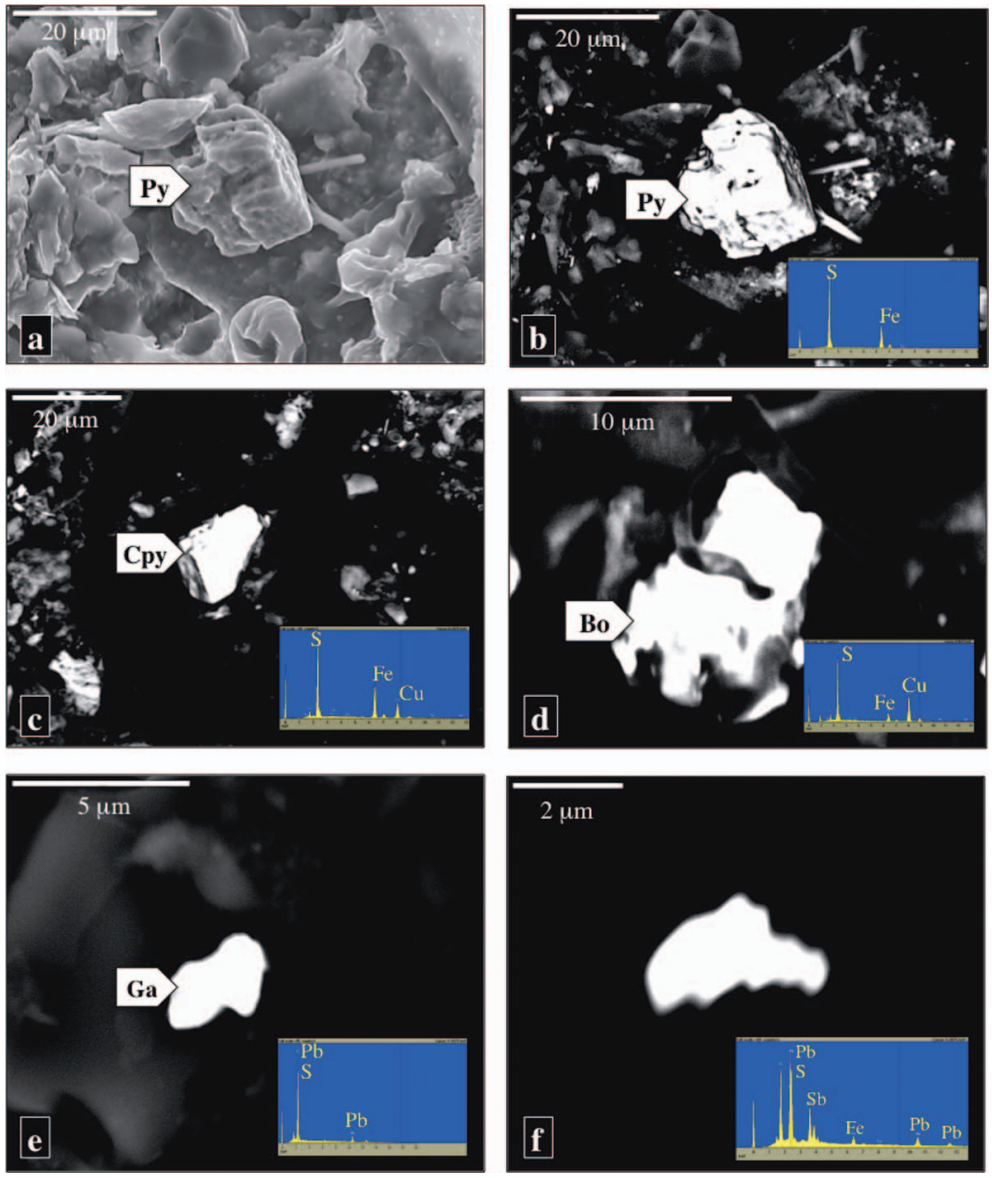

FIG. 6. SEM photomicrographs and EDS spectra of some primary metal sulfides found in the dustfall: SE (*a*) and BSE (*b*) images of a partially dissolved crystal of pyrite; (*c*) subhedral crystal of chalcopyrite; (*d*) particle of copper-iron sulfide ascribed to bornite; (*e*) irregular rounded particle of galena; (*f*) small particle of lead-antimony sulfosalt. Mineral abbreviatons: Bo: bornite; Cpy: chalcopyrite; Ga: galena; Py: pyrite.

crystals with a very sharp hexagonal contour, as well as porous irregular aggregates of sub-micron sized particles. It must be noted that the SEM-EDS analysis indicated the presence of detectable amounts of Pb in the aggregates of jarosite.

The abundance of iron oxy-hydroxides and jarosite group minerals in the dustfall, even at levels detectable by XRD in the case of the goethite, can be explained by the widespread occurrence of such oxidation products of pyrite

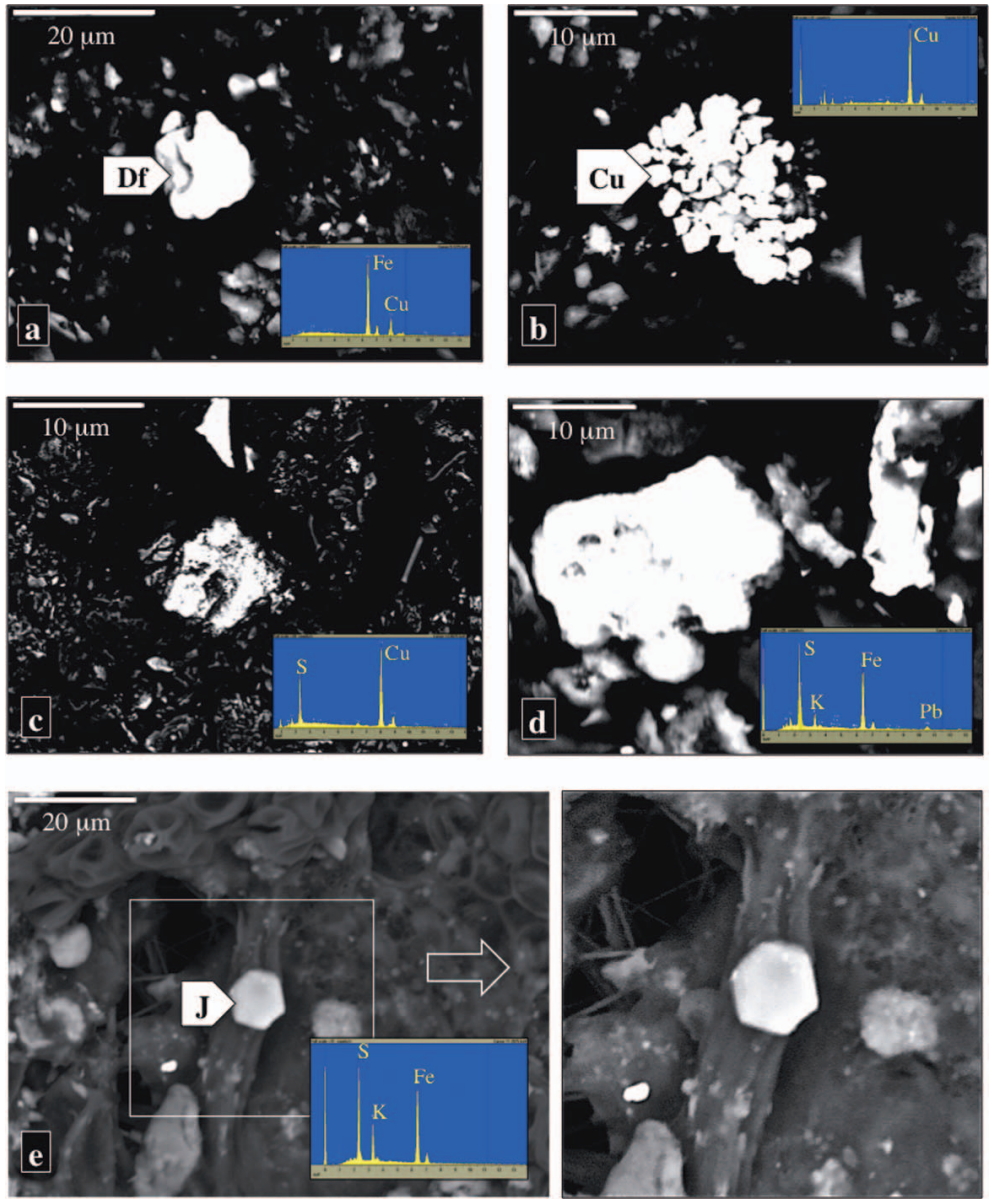

FIG. 7. SEM images and EDS spectra of some secondary metal-bearing minerals found in the dustfall: (*a*) subspheric particle of delafossite; (*b*) cluster of copper oxide particles ascribed to cuprite; (*c*) aggregate of copper sulfide, probably chalcocite or covellite; (*d*) aggregate of Pb-bearing jarosite (plumbojarosite); (*e*) well formed pseudohexagonal crystal of jarosite. Mineral abbreviatons: Cu: cuprite; Df: delafossite; J: jarosite.

not only in the oxidizing environment of the mine wastes but also in soils, sediments and iron-rich residual deposits (gossan) that remain unexploited in the area. This mineral association can be used as a tracer for identifying local dust source areas and major transportation routes of airborne particles dispersed from the mine land.

Finally, discrete particles of copper sulfides were also identified in several samples. Although some of these airborne particles may contain

detectable levels of Fe and As, particularly in dustfall samples collected at the RTF station, they might correspond to crystals of chalcocite or covellite.

Metallic compounds of anthropogenic origin

Individual particles or, more often, complex aggregate dust particles chemically composed of various metals such as Fe, Cr, Mn, Ni and/or Zn were recognized in all the samples collected at the CTR station. Electron microscope observations showed that the constituent particles of the aggregates display globular or ball-like morphologies with sizes ranging up to a few microns (Fig. 8). The great relative abundance of these settled micron-sized particles in samples from the

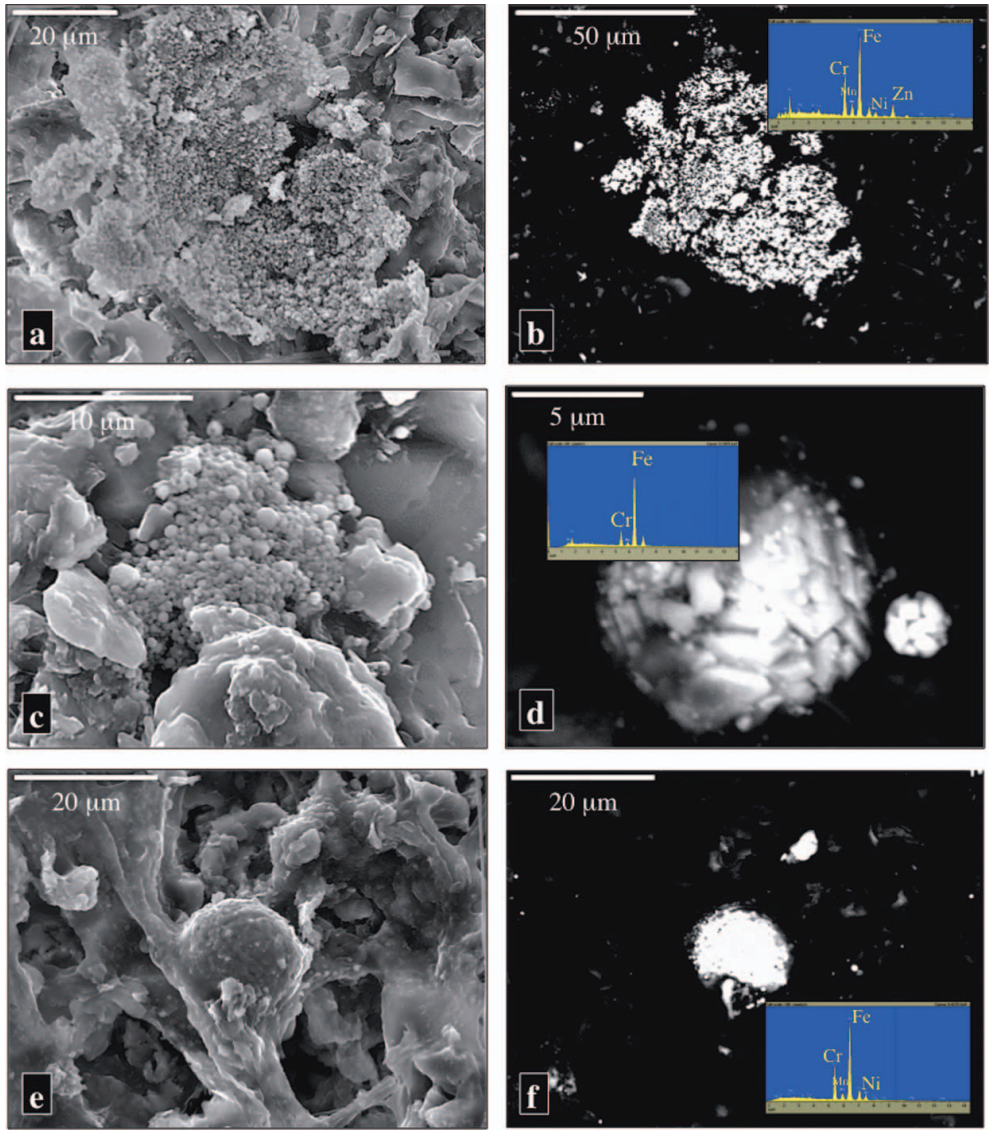

FIG. 8. SE (*a*) and BSE (*b*) images and EDS spectrum of anthropogenic metal-bearing phases found in the dustfall samples collected at CTR station; (*c*) dust aggregates consisting of sphere-like particles containing significant amounts of Fe, Cr and Zn, with minor Mn and Ni; (*d*) spherical aggregate of Fe- and Cr-rich micron-sized particles; (*e–f*) globular aggregate bearing Fe, Cr, Ni and Mn.

CTR station is consistent with the analytical results of the present study concerning the relatively high levels of Zn, Cr and Ni in the dustfall deposition detected in the same samples.

Interestingly, because of the small concentrations of Cr, Mn and Ni in the polymetallic ores of the Rio Tinto deposits, as well as in wastes from mining and smelting operations, there is need to seek another anthropogenic source for these metallic air pollutants. At this point, it is important to note that CTR is the sampling site closest to the centre for hazardous waste management where steelworks dust has been landfilled. Therefore, the most plausible local source for Ni and Cr could be fugitive particulates emissions from waste disposal operations.

Environmental implications

Although there is evidence that trace elements do not contribute greatly to total mass deposition (the annual fluxes of the bulk deposition registered in the Rio Tinto mining district are between 18,000 and 43,000 mg/m^2 according to Castillo *et al.*, 2013), some metals were to be found at a level which may be of ecotoxicological relevance for human health and the environment. In fact, dispersal of deflated dust and fugitive emissions of inhalable particles (<10 μm in aerodynamic diameter), in particular when they contain potentially harmful metals and metalloids, contributes to health hazards in the area as documented by Sánchez de la Campa *et al.* (2011).

A further impact to be considered is that caused by atmospheric deposition of coarse and supercoarse (>10 μm) particles of metallic sulfides and oxides onto the landscape surface. These mineral species are the most important carriers of metals in the settleable particulate matter, and provide supporting evidence for a link between metal-bearing airborne particles and sulfides that have not yet been oxidized and are present in agricultural soils surrounding Rio Tinto and other mining sites of the Iberian Pyrite Belt (Fernández-Caliani and Barba-Brioso, 2010; Madejón *et al.*, 2011). Thus, a remarkable proportion of trace elements found in topsoils around the Rio Tinto mines (Chopin and Alloway, 2007*a*,*b*; López *et al.*, 2008; Fernández-Caliani *et al.*, 2009) could have been removed from the atmosphere by gravitational settling after a short residence period in the air, due to the large particle size of the heavy-metal bearing particles in suspension.

Atmospheric deposition may also be an important source of potentially phytotoxic metals to agricultural plants. Unwashed leaf samples from citrus trees neighbouring the mines have been reported to accumulate higher levels of metals, especially Cu, than those found in washed leaves (Romero *et al.*, 2012). Accordingly, metals do not seem to be bioassimilated by the plant, via foliar absorption or root uptake, but rather they occur as tiny dust metal-bearing particles coating the leaves of the citrus trees.

Finally, note that metals and metalloids, particularly those bound to reactive sulfides (notably pyrite), are deposited in a potentially mobile form. Under the oxidizing conditions prevailing in mine soils, the sulfide particles tend to dissolve leading to the formation of acid sulfate soils (Nordstrom, 1982), and thus increasing the concentrations of bioavailable metals in the soil solution.

Concluding remarks

This study has shown that the mineral composition and particle size of atmospheric dustfall are important criteria for recognizing air pollution sources. Dust deposited in the Rio Tinto mining district is composed of a variety of metal-bearing accessory minerals, the most common being pyrite and its oxidation products (iron oxyhydroxides and jarosite), suggesting a dominant local source of wind-blown dust.

The atmospheric bulk (wet plus dry) deposition of trace elements varied depending on various factors: (1) the type of metal or metalloid; (2) the location of the sampling station; and (3) the sampling period. High deposition levels of sulfide-related metals (As, Bi, Cd, Cu, Pb, Sb, Zn) were registered at the sampling station adjacent to the mine waste dumps, so that the mining district also displays a local signature of atmospheric metal deposition. It can be concluded, therefore, that heavy-metal bearing particles removed by wind from the abandoned mine wastes have been a persistent source of air pollution in the area. However, local dust generation is not restricted to mine wastes. Steelworks' dust arising from the hazardous waste disposal centre may be making a relevant contribution to the metal flux deposition, particularly for Fe, Ni, Cr and Mn.

Another interesting conclusion drawn from the study is that atmospheric deposition is a major

mechanism for metal input to soils and plants. Future research efforts should be addressed to improving our understanding of the processes involved in the atmospheric dispersal of metal-bearing particles, the environmental fate of metals, and their potential transference throughout the food web.

Acknowledgements

This study was supported by grants from the Spanish Ministry of Science and Innovation (Projects CRACCIE-CSD2007-0067 and CGL2008-06270-C02-02/CLI) and the Department of the Environment, and the Department of Innovation, Science and Enterprise (Projects RNM2007-02729 and RNM2009-5163M) of the Andalusia Autonomous Government. Karen Hudson-Edwards and an anonymous reviewer are thanked for their constructive comments and suggestions.

References

Azimi, S., Ludwig, A., Thévenot, D.R. and Colin, J.L. (2003) Trace metal determination in total atmospheric deposition in rural and urban areas. *Science of the Total Environment*, **308**, 247–256.

Castillo, S., De la Rosa, J.D., Sánchez de la Campa, A.M., González-Castanedo, Y., Fernández-Caliani, J.C., González, I. and Romero, A. (2013) Contribution of mine wastes to atmospheric metal deposition in the surrounding area of an abandoned heavily polluted mining district (Rio Tinto mines, Spain). *Science of the Total Environment*, **449**, 363–372.

Chopin, E.I.B. and Alloway, B.J. (2007*a*) Trace element partitioning and soil particle characterisation around mining and smelting areas at Tharsis, Riotinto and Huelva, SW Spain. *Science of the Total Environment*, **373**, 488–500.

Chopin, E.I.B. and Alloway, B.J. (2007*b*) Distribution and mobility of trace elements in soils and vegetation around the mining and smelting areas of Tharsis, Riotinto and Huelva, Iberian Pyrite Belt, SW Spain. *Water Air and Soil Pollution*, **182**, 245–261.

Csavina, J., Field, J., Taylor, M.P., Gao, S., Landázuri, A., Betterton, E.A. and Eduardo, A. (2012) A review on the importance of metals and metalloids in atmospheric dust and aerosol from mining operations. *Science of the Total Environment*, **433**, 58–73.

Fernández-Caliani, J.C. and Barba-Brioso, C. (2010) Metal immobilization in hazardous contaminated minesoils after marble slurry waste application. A field assessment at the Tharsis mining district (Spain). *Journal of Hazardous Materials*, **181**, 817–826.

Fernández-Caliani, J.C. and Galán, E. (1996) Impacto ambiental de la minería en el devenir histórico de la comarca de Riotinto (Huelva). *Geogaceta*, **20**, 1168–1169.

Fernández-Caliani, J.C., Barba-Brioso, C., Gonzalez, I. and Galán E. (2009) Heavy metal pollution in soils around the abandoned mine sites of the Iberian Pyrite Belt (Southwest Spain). *Water Air and Soil Pollution*, **200**, 211–226.

Fernández-Remolar D.C., Prieto-Ballesteros, O., Gómez-Ortiz, D., Fernández-Sampedro, M., Sarrazin, P., Gailhanou, M. and Amils, R. (2011) Rio Tinto sedimentary mineral assemblages: A terrestrial perspective that suggests some formation pathways of phyllosilicates on Mars. *Icarus*, **211**, 114–138.

Galán, E., Gómez-Ariza, J.L., González, I., Fernández-Caliani, J.C., Morales, E. and Giráldez, I. (2003) Heavy metal partitioning in river sediments severely polluted by acid mine drainage in the Iberian Pyrite Belt. *Applied Geochemistry*, **18**, 409–421.

García-Palomero, F. (1980) *Caracteres Geológicos y Relaciones Morfológicas y Genéticas de los Yacimientos del Anticlinal de Riotinto*. Instituto de Estudios Onubenses, Diputación Provincial de Huelva.

Golomb, D., Ryan, D., Eby, N., Underhill, J. and Zemba S. (1997) Atmospheric deposition of toxic onto Massachusetts Bay – I. Metals. *Atmospheric Environment*, **31**, 1349–1359.

Kahle, M., Kleber, M. and Reinhold, J. (2002) Review of XRD-based quantitative analyses of clay minerals in soils: the suitability of mineral intensity factors. *Geoderma*, **109**, 191–205.

López, M., González, I. and Romero, A. (2008) Trace elements contamination of agricultural soils affected by sulphide exploitation (Iberian Pyrite Belt, SW Spain). *Environmental Geology*, **54**, 805–818.

Lottermoser, B.G. (2005) Evaporative mineral precipitates from a historical smelting slag dump, Rio Tinto, Spain. *Neues Jahrbuch fur Mineralogie*, **181**, 183–190.

Lottermoser, B.G. (2010) *Mine Wastes. Characterization, Treatment, Environmental Impacts* 3rd Edition, Springer-Verlag, Berlin.

Madejón, P., Barba-Brioso, C., Lepp, N.W. and Fernández-Caliani, J.C. (2011) Traditional agricultural practices enable sustainable remediation of highly polluted soils in Southern Spain for cultivation of food crops. *Journal of Environmental Management*, **92**, 1828–1836.

Meza-Figueroa, D., Maier, R.M., De la O-Villanueva, M., Gomez-Alvarez, A., Moreno-Zazueta, A., Rivera

J., Campillo A., Grandlic C.J., Anaya R., and Palafox-Reyes J. (2009) The impact of unconfined mine tailings in residential areas from a mining town in a semi-arid environment: Nacozari, Sonora, Mexico. *Chemosphere*, **77**, 140–147.

Moreno, T., Oldroyd, A., McDonald, I. and Gibbons, W. (2007) Preferential fractionation of trace metals-metalloids into PM_{10} resuspended from contaminated gold mine tailings at Rodalquilar, Spain. *Water Air and Soil Pollution*, **179**, 93–105.

Nordstrom, D.K. (1982) Aqueous pyrite oxidation and the consequent formation of secondary iron minerals. Pp. 37–56 in: *Acid Sulfate Weathering* (J.A. Kittrick, D.S. Fanning and L.R. Hossner, editors). Soil Science Society of America, Madison, Wisconsin, USA.

Plumlee, G.S. and Morman, S.A. (2011) Mine wastes and human health. *Elements*, **7**, 399–404.

Querol, X., Alastuey, A., Rodríguez, S., Plana, F., Ruiz, C.R., Cots, N., Massagué, G. and Puig, O. (2001) PM10 and PM2.5 source apportionment in the Barcelona Metropolitan Area, Catalonia, Spain. *Atmospheric Environment*, **35**, 6407–6419.

Rasmussen, P.E. (1998) Long-range atmospheric transport of trace metals: the need for geoscience perspectives. *Environmental Geology*, **33**, 96–108.

Roberts, R.D. and Johnson, M.S. (1978) Dispersal of heavy metals from abandoned mine workings and their transference through terrestrial food chains. *Environmental Pollution*, **16**, 293–310.

Romero, A., González, I. and Galán E. (2006) Estimation of potential pollution of waste mining dumps at Peña de Hierro (Pyrite Belt, SW Spain) as a base for future mitigation actions. *Applied Geochemistry*, **21**, 1093–1108.

Romero, A., González, I. and Galán, E. (2012) Trace elements absorption by citrus in a heavily polluted mining site. *Journal of Geochemical Exploration*, **113**, 76–85

Salkield, L.U. (1987) *A Technical History of the Rio Tinto Mines. Some Notes on Exploitation from Pre-Phoenician Times to the 1950s*. Institution of Mining and Metallurgy, London.

Sánchez de la Campa, A.M., De la Rosa, J.D., Fernández-Caliani, J.C. and González-Castanedo, Y. (2011) Impact of abandoned mine waste on atmospheric respirable particulate matter in the historic mining district of Rio Tinto (Iberian Pyrite Belt). *Environmental Research*, **111**, 1018–1023.

Zota, A.R., Willis, R., Jim, R., Norris, G.A., Shine, J.P., Duvall, R.M., Schaider, L.A. and Spengler, J.D. (2009) Impact of mine waste on airborne respirable particulates in northeastern Oklahoma, United States. *Journal of the Air & Waste Management Association*, **59**, 1347–1357.